UNIVERSITATEA "BABEŞ-BOLYAI" CLUJ-NAPOCA
FACULTATEA DE FIZICĂ
SPECIALIZAREA FIZICĂ COMPUTAŢIONALĂ

LUCRARE DE DISERTAŢIE

Coordonator ştiinţific
Dr. Nagy Ladislau

Absolvent
Bálint Zsuzsánna

2025

UNIVERSITATEA "BABEŞ-BOLYAI" CLUJ-NAPOCA
FACULTATEA DE FIZICĂ
SPECIALIZAREA FIZICĂ COMPUTAŢIONALĂ

LUCRARE DE DISERTAŢIE

EXCITATION OF HELIUM BY PROTON AND ANTIPROTON IMPACT

Coordonator ştiinţific
Dr. Nagy Ladislau

Absolvent
Bálint Zsuzsánna

2025

ABSTRACT

The present study focuses on the excitation of helium by proton and antiproton impact. Excitation cross sections for proton-helium and antiproton-helium collisions have been calculated. Two computational approaches have been employed: a first-order perturbational calculation and an ab initio calculation, where the time-dependent Schrödinger equation is solved numerically for the two-electron system. A comparison of these two approaches reveals the importance of electron correlations and higher-order effects. In addition, the influence of the projectile charge sign on the excitation cross section is studied.

Contents

Introduction

The excitation of helium by proton impact has been a subject of both experimental and theoretical study for a considerable period. Conversely, theoretical studies of excitation due to antiproton impact remain scarce. This is in contrast to the case of ionization, for which several groups have investigated and compared the cross sections for proton and antiproton projectiles, discussing the effect of the projectile's charge sign.

In the present work, the excitation cross sections of helium atoms in collision with proton and antiproton projectiles are calculated. The present study employs two distinct computational approaches: an ab initio, time-dependent close-coupling (TDCC) calculation, based on the numerical solution of the time-dependent Schrödinger equation for two electrons, and a simpler, first-order perturbative calculation. A comparison of the results obtained from different approaches can reveal the importance of higher-order and electron correlation effects in these excitation processes, and clearly show the limits of the applicability of the first-order calculations for different excited states in different energy impact regions. While the first-order calculation leads to the same cross section for protons and antiprotons, the ab initio calculation shows that the excitation cross section depends on the sign of the projectile charge, and can reveal the cause of these differences (higher-order effects such as target polarization, electron correlation). A comparison is made between the present results for proton impact and previous calculations, as well as existing experimental data. For the antiproton impact, a comparison is made with the few existing theoretical excitation cross sections. This study intends to contribute to a better understanding of two-electron dynamics in the ion–atom collision processes.

My contribution to the project entails the development of the software utilised for the perturbation calculations, in addition to the analysis and visualisation of the data. It is important to note that all figures and the data presented on them are part of the original results, except for comparisons where the source of the data used to create the figure is referenced.

In Chapter 1, we provide a comprehensive overview of the field of helium excitation study. In Chapter 2, the theoretical and computational methods are presented. In Chapter 3, the results obtained from this study are presented and compared with those of other models and experiments.

Throughout this work, we use atomic units (a.u.) unless stated otherwise. These units are defined as follows:

$$
\begin{aligned}
e &= 1 \text{ a.u. of charge,} \\
m_e &= 1 \text{ a.u. of mass,} \\
\hbar &= 1 \text{ a.u. of angular momentum,} \\
a_0 &= 1 \text{ a.u. of length,}
\end{aligned}
$$

where e is the absolute value of the electron charge, m_e is the electron mass, $\hbar = \frac{h}{2\pi}$ is the reduced Planck's constant and a_0 is the Bohr radius. The electrostatic constant $4\pi\epsilon_0$ is also equal to 1.

This research has been published in the peer-reviewed journal *Atoms* (see citation [1]).

Chapter 1

Description of the Field

Cross sections of the excitation of helium via proton impact have been experimentally measured and calculated since the 1960's; for example, see the articles by Thomas [2, 3] and the references therein. Obtaining these data has been particularly interesting for modelling fusion plasma, which was still a focus within the field in the 1990s [4, 5]. On the other hand, to our knowledge there are no experimental data on the excitation of helium by antiproton projectiles. However, since 1987 several measurements have been made for the single and double ionization of helium by antiproton impact and the cross sections obtained have been compared with the corresponding proton data [6]. As expected, the effect of the projectile's charge sign on the result was small in the case of single ionization. However, for double ionization, the cross section of the antiproton's impact was much higher than that of the corresponding proton impact. This result explained the previously observed Barkas effect for the stopping power of positively and negatively charged projectiles in matter. The dependence of the double ionization cross section on the charge sign was explained by the importance of electron correlation and the interference between first-order and second-order contributions [7, 8, 9]. Since then, several more precise experimental measurements and calculations have been performed for the ionization of helium by antiproton impact [10, 11, 12, 13, 14, 15, 16, 17, 18, 19, 20, 21], but the excitation process has generally been neglected. Some calculations were published for proton impact [22, 23, 24], and even for antiproton impact [25, 26, 27, 28], the focus was not on the excitation processes. As such, we have no knowledge about experimental cross sections for antiproton impact.

Chapter 2

Theoretical Background

In our calculations, we use the semi-classical impact parameter approximation, which assumes a classical straight-line trajectory for the projectile, and only the electron system of the target is treated using quantum mechanics. This approach is valid for fast, heavy projectiles such as protons or antiprotons, for which the de Broglie wavelength is negligible compared to atomic dimensions. Deviations from the straight-line trajectory because of Coulomb deflection from the nucleus are negligible. In the case of the lowest considered projectile energy (100 keV), the deviation is greater than 1° only for impact parameters lower than 0.05 atomic units. This region contributes to a cross section of less than 0.1%.

Furthermore, the validity of the straight-line trajectory model was also demonstrated by Classical Trajectory Monte Carlo (CTMC) calculations for projectiles with even lower energies, down to 3 keV [20]. This semi-classical model cannot be applied to equivelocity light projectiles (electrons and positrons). In those cases, the de Broglie wavelength associated with the projectile is close to atomic dimensions, so a classical description would be incorrect, and a quantum description is needed, as in [29].

The cross section can be expressed as an integral over the impact parameter $\mathbf{b}$

$$\sigma_{i\to f} = \int d^2\mathbf{b}|a_{i\to f}|^2. \tag{2.1}$$

Here $a_{i\to f}$ is the transition probability amplitude and i and f represent the initial and final states (i.e. eigenstates of the unperturbed Hamiltonian of the atomic system with energies E_i and E_f, respectively). The transition probability is given by

$$w_{i\to f} = |a_{i\to f}|^2. \tag{2.2}$$

2.1 Perturbational Method

To solve the time-dependent Schrödinger equation

$$i\frac{\partial}{\partial t}\Psi(\mathbf{r_1},\mathbf{r_2},t) = \hat{H}\Psi(\mathbf{r_1},\mathbf{r_2},t), \tag{2.3}$$

we first use a perturbational method. The simplest way to calculate the excitation cross section is the application of one active electron and first-order perturbation approximation. The projectile trajectory is assumed to be along the Oz axis. As shown in Appendix A, in this framework the first-order transition amplitude is calculated as the integral of the matrix element of the projectile–electron interaction (multiplied by an oscillating factor) over the z coordinate (the trajectory) of the projectile

$$a^{(1)} = i\frac{Z_p}{v}\int_{-\infty}^{\infty} dz\, e^{i\frac{E_f-E_i}{v}z}\left\langle f\left|\frac{1}{|\mathbf{R}(t)-\mathbf{r}|}\right|i\right\rangle. \tag{2.4}$$

Here, $\mathbf{r}$ is the position vector of the active electron, Z_p is the charge and v is the velocity of the projectile. E_i and E_f are the energies of eigenstates i and f, respectively. $\mathbf{R}(t)$ is the position vector of the projectile expressed as

$$\mathbf{R}(t) = \mathbf{b} + \mathbf{v}\cdot t, \tag{2.5}$$

where $\mathbf{b}$ is the impact parameter and $\mathbf{v}$ is the velocity vector of the projectile.

For the single-electron wave functions i and f, the radial and orbital parts are separated

$$i = R_i(r)\,Y_{l_i m_i}(\hat{\mathbf{r}}), \tag{2.6}$$

$$f = R_f(r)\,Y_{l_f m_f}(\hat{\mathbf{r}}). \tag{2.7}$$

Here, l_i, l_f, m_i and m_f are the orbital and magnetic quantum numbers of the active electron in the initial and final states, respectively.

The interaction potential is expanded using the multipole series

$$\frac{1}{|\mathbf{R}(t)-\mathbf{r}|} = \sum_{l=0}^{\infty}\frac{r_<^l}{r_>^{l+1}}P_l(\cos\theta), \tag{2.8}$$

where the Legendre polynomial depends on the mutual angle between $\mathbf{r}$ and $\mathbf{R}$, while $r_< = \min\{|\mathbf{r}|,|\mathbf{R}|\}$ and $r_> = \max\{|\mathbf{r}|,|\mathbf{R}|\}$.

In order to perform the integral according to the orbital coordinates of the electron, we

make use of the expression of the Legendre polynomials as a function of spherical harmonics

$$P_l(\cos\theta) = \frac{4\pi}{2l+1}\sum_{m=-l}^{l} Y^*_{lm}(\hat{\mathbf{R}})Y_{lm}(\hat{\mathbf{r}}). \tag{2.9}$$

Substituting (2.6)–(2.9) into expression (2.4) of the transition amplitude, we perform the integration over $\hat{\mathbf{r}}$ using the equation

$$\int Y^*_{l_f m_f}(\hat{\mathbf{r}})Y_{lm}(\hat{\mathbf{r}})Y_{l_i m_i}(\hat{\mathbf{r}})\,d\hat{\mathbf{r}} = \sqrt{\frac{(2l+1)(2l_i+1)}{4\pi(2l_f+1)}}C^{l_f 0}_{l0l_i 0}C^{l_f m_f}_{lml_i m_i}, \tag{2.10}$$

where $C^{l_f 0}_{l0l_i 0}$ and $C^{l_f m_f}_{l_i m_i lm}$ are the Clebsch–Gordan coefficients. For the first-order excitation amplitude, we obtain

$$\begin{aligned} a^{(1)} = i\frac{Z_p}{v}\sum_l \frac{4\pi}{2l+1}\sqrt{\frac{(2l_i+1)(2l+1)}{4\pi(2l_f+1)}}C^{l_f 0}_{l_i 0l0}\sum_m C^{l_f m_f}_{l_i m_i lm}\times \\ \int_{-\infty}^{+\infty} dz\, e^{i\frac{E_f-E_i}{v}z}Y^*_{lm}(\hat{\mathbf{R}})\int_{-\infty}^{+\infty} dr\, r^2 R^*_f(r)\frac{r^l_<}{r^{l+1}_>}R_i(r). \end{aligned} \tag{2.11}$$

The summation over the angular momentum l ranges from $|l_i - l_f|$ to $l_i + l_f$, while the magnetic quantum number m is determined $m = m_f - m_i$.

Substituting (2.11) into (2.1) yields a multidimensional integral in $\mathbf{b}$, z and $\mathbf{r}$. Convergence tests were carried out for the boundaries and step sizes in these integrals to ensure the accuracy of the obtained results.

2.2 The Time-Dependent Close-Coupling Method

In our ab initio approach, the quantum dynamics of the two active electrons driven by the time-dependent Coulomb field of the classical projectile are solved numerically using the TDCC method [19]. The fully correlated two-electron wave function is represented as

$$\Psi(\mathbf{r_1}, \mathbf{r_2}, t) = \sum_{l_1 l_2 LM}\frac{R^{LM}_{l_1 l_2}(r_1, r_2, t)}{r_1 r_2}\Upsilon^{LM}_{l_1 l_2}(\Omega_1, \Omega_2) \tag{2.12}$$

in the basis of symmetrized coupled spherical harmonics [20, 21]

$$\Upsilon^{LM}_{l_1 l_2}(\Omega_1, \Omega_2) = \frac{1}{\sqrt{2+2\delta_{M0}}}\left[Y^{LM}_{l_1 l_2}(\Omega_1, \Omega_2) + (-1)^{l_1+l_2+L+M}Y^{L-M}_{l_1 l_2}(\Omega_1, \Omega_2)\right]. \tag{2.13}$$

Substituting (2.12) into (2.3) leads to the TDCC equations, which are a system of coupled partial differential equations in $(\mathbf{r_1}, \mathbf{r_2}, t)$.

For the radial partial wave functions $R^{LM}_{l_1 l_2}(r_1, r_2, t)$ we have used the finite element discrete variable representation (FEDVR) [30, 31], where each radial coordinate is divided into finite elements (i.e., segments with finite length) and inside each finite element the wave function is represented on a local polynomial basis. For the time propagation of the wave function, the short iterative Lanczos method [32, 33] with adaptive time step control was implemented.

The time evolution of the wave function was started from the ground state of He, which in turn was obtained by performing the negative imaginary time propagation ($t \to -i\tau$) of an initial guess wave function.

The excitation probability amplitudes were calculated directly from the time-dependent wave function by projecting it onto eigenstates of the He target obtained by directly diagonalizing the discretized Hamiltonian using the Scalable Library for Eigenvalue Problem Computations (SLEPc) package [34]. Convergence tests were carried out with regard to the numerical parameters of the model, i.e. the size and density of the FEDVR grid, the simulated length of the projectile trajectory and the size of the angular basis. These tests ensured the accuracy of the obtained results.

Chapter 3

Results and Discussion

We have performed calculations for the excitation of helium by proton and antiproton impact in the projectile energy region between 100 and 1000 keV. In the case of the ab initio calculations, the two-electron wave functions for the initial and final states were obtained by our code, but for the perturbational calculations we have used one-electron variational wavefunctions from the literature. The $1s$ ground state is taken from the basic configuration of the wavefunction of Nesbet and Watson [35], while for the $2s$ and $2p$ excited states we have used the wavefunctions given in [36]. The $3d$ excited state is taken to be simply a hydrogenlike function. The $2s$ wavefunction is orthogonalized onto the ground state using the Gram–Schmidt method.

In addition to excitation cross sections (comparable with experiments), we also show transition probabilities as a function of the impact parameter in order to identify the impact parameter regions in which the first-order calculations fail.

3.1 Transition probabilities

The impact parameter dependence of the excitation probabilities in the $2s$ state obtained from the perturbational method and the ab initio calculations are presented in Figure 3.1, where the impact parameter is in atomic units (a.u.).

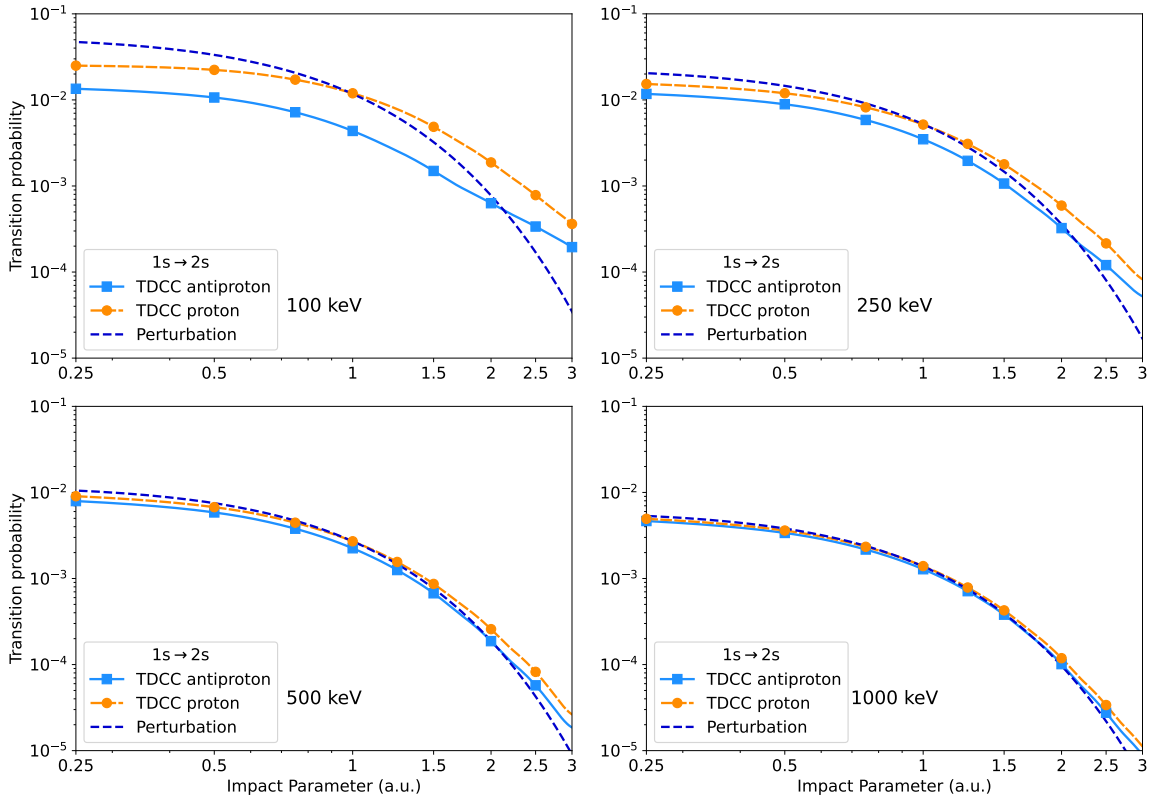

Figure 3.1: Transition probabilities for the $1s \rightarrow 2s$ excitation process of helium as a function of the impact parameter for proton and antiproton projectiles in the case of different impact energies. The results obtained from the ab initio TDCC calculations are presented compared to the first-order perturbational approximation.

For the highest projectile energy (1000 keV), as expected, the results obtained with the perturbational method are in good agreement with the TDCC calculations, and there is no significant difference between the transition probabilities for protons and antiprotons. For lower impact energies, the higher-order and electron correlation effects become more and more important, and the difference between the two methods increases. We obtained higher transition probabilities for protons than for antiprotons for all impact parameters. This may be caused by the fact that the protons attract the electrons, resulting in a smaller average electron–projectile distance and a stronger interaction during the collision. The first-order results are higher than the ab initio data for small impact parameters in the case of both projectiles.

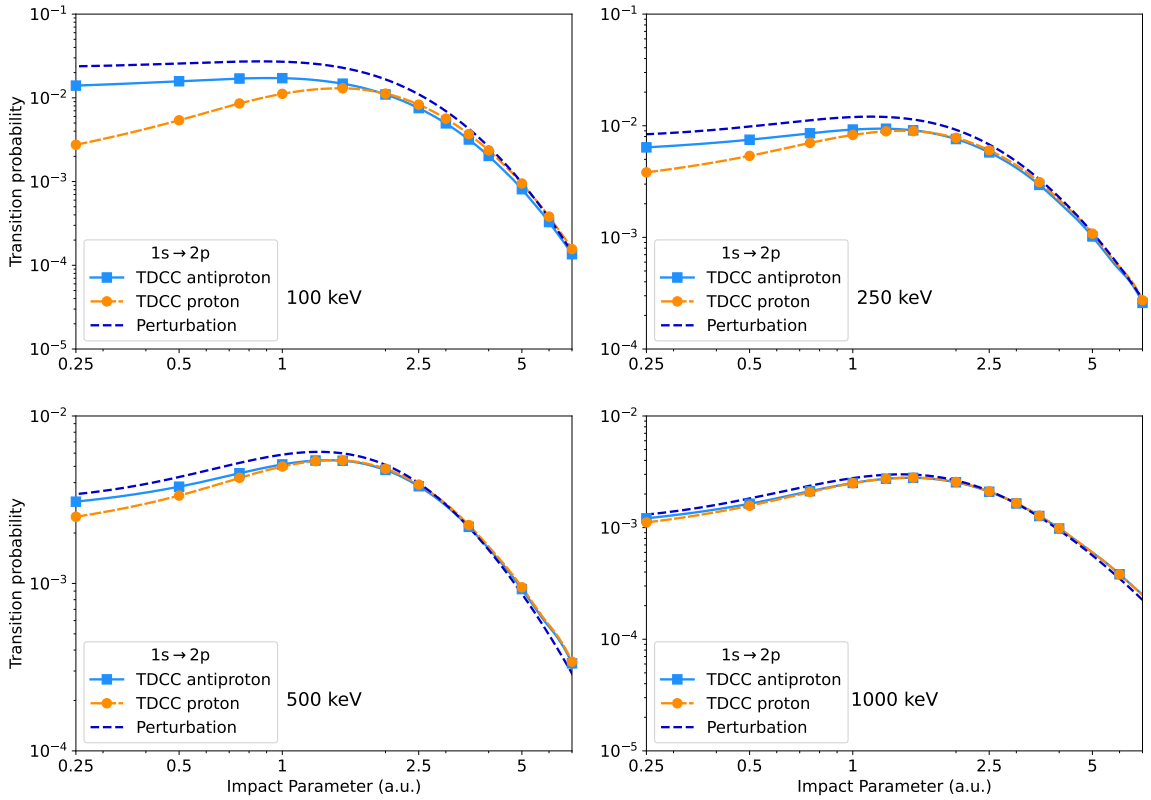

Figure 3.2: Same as Figure 3.1 but for the $1s \rightarrow 2p$ transition.

The $1s \rightarrow 2p$ excitation probabilities calculated with the perturbational approximation and the TDCC method are shown in Figure 3.2. Similar to the $1s \rightarrow 2s$ excitation, for the highest impact energy the transition probability practically does not depend on the charge sign of the projectile, and the perturbational approach gives comparable results. For lower impact energies, the difference between the three curves increases, particularly for small impact parameters. In the case of large impact parameters, where the distant collision mechanism is dominant [37], the perturbational result reproduces those obtained from the ab initio calculations very well. This suggests that, in this impact parameter region, the excitation is mainly a single-electron process and the electron correlation effects can be neglected, even at 100 keV projectile energy. In contrast, significant differences are observed in the proton- and antiproton-induced transition probabilities at small impact parameter values. This indicates that in the excitation process the correlated multi-particle quantum dynamics plays an important role, which is the fingerprint of the close collision mechanism [37]. An important difference relative to the $1s \rightarrow 2s$ excitation is that, in the present case, the transition probabilities for antiprotons and for small impact parameters (below 1 a.u.) are much higher than for protons. For impact parameters above 2 a.u., the transition probabilities for antiprotons are slightly smaller compared to proton projectiles.

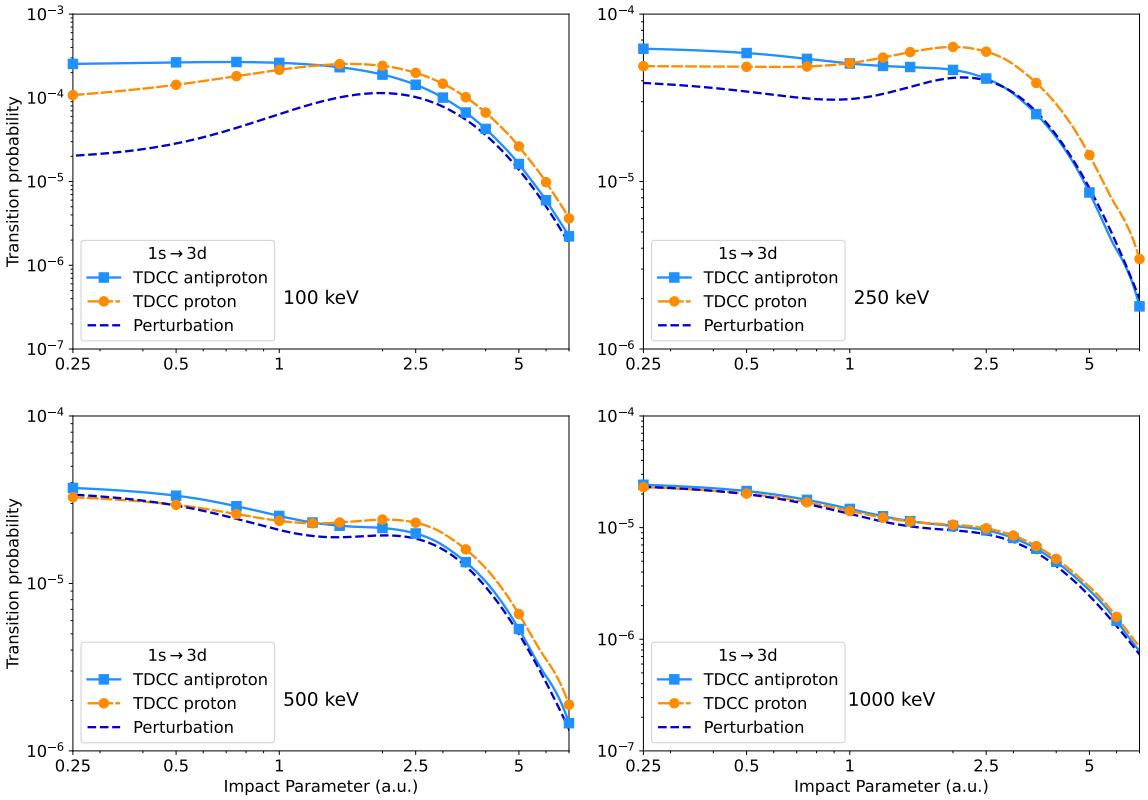

Figure 3.3: Same as Figure 3.1 but for the $1s \rightarrow 3d$ transition.

The $1s \rightarrow 3d$ excitation probabilities calculated using the TDCC and the perturbational method are shown in Figure 3.3. Similarly to the previous cases, for a 1000 keV projectile energy the transition probabilities are practically the same for protons and antiprotons, and the first-order approximation reproduces the TDCC results well. For lower impact energies, the TDCC method leads to higher excitation probabilities for antiprotons than for proton projectiles below the impact parameter $b = 1$, and higher transition probabilities for protons at larger impact parameters. The perturbational method underestimates the results especially for small impact parameters, and at 100 and 250 keV projectile energies.

3.2 Excitation cross sections

The excitation cross sections for the $1s \rightarrow 2s$ transition are presented in Figure 3.4 for proton (left panel) and antiproton (right panel) projectiles as a function of impact energy. Our TDCC and perturbational results are compared with the theoretical calculations for protons by Alladustov et al. [23], and for antiprotons with the calculations by Igarashi et al. [27] and the coupled pseudostate (CP) results of McGovern et al. [28]. We also show the recommended values proposed for proton projectiles by Heer et al. [5]. Our TDCC results show a good overall agreement with these data for both projectiles, but for lower proton energies we obtain up to 10% smaller cross sections than the recommended values. The first-order results are close to the ab initio ones for proton projectiles even at the lowest energy, while they overestimate the cross sections obtained with antiprotons up to a factor of 2.2 at 100 keV. This observation suggests that, for this transition, electron correlation and higher-order effects are more important for antiprotons than for protons.

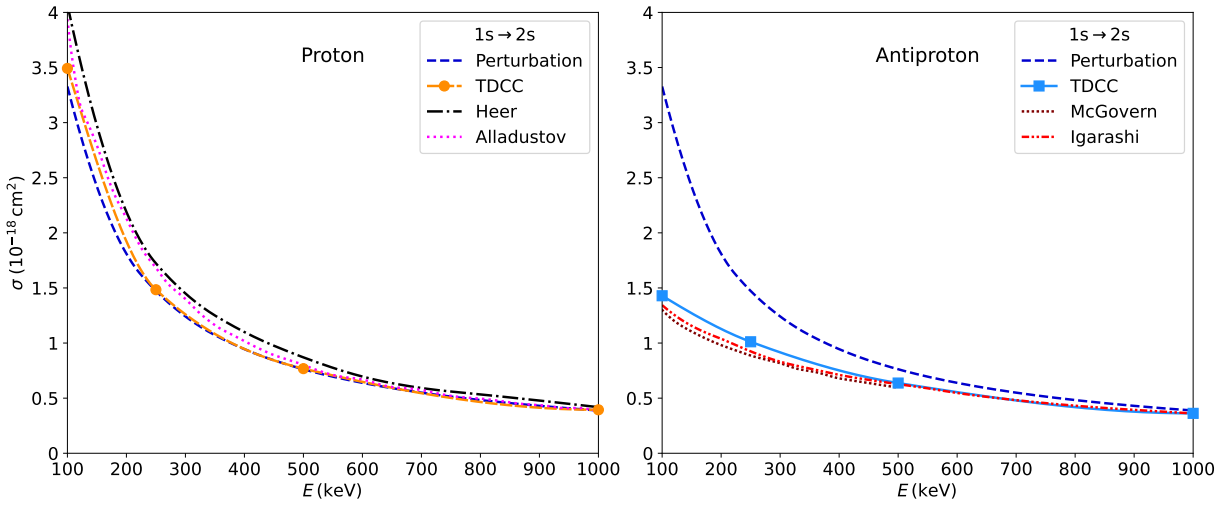

Figure 3.4: Excitation cross sections of helium for the $1s \rightarrow 2s$ transition as a function of the projectile energy for proton (**left panel**) and antiproton (**right panel**) projectiles. The results of the first-order perturbation approximation and the TDCC method are compared with the recommended values given by Heer et al. [5] and the theoretical results of Alladustov et al. [23] for proton projectiles, and the calculations of Igarashi et al. [27] and McGovern et al. [28] for antiproton projectiles.

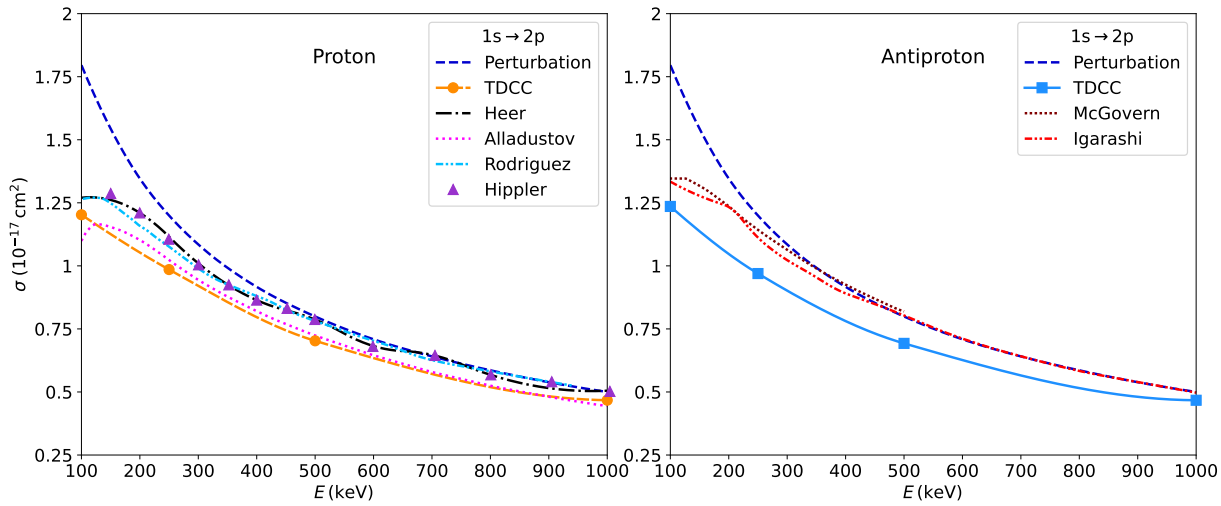

Figure 3.5: Same as Figure 3.4, but for the $1s \rightarrow 2p$ transition. The results for protons are compared in addition to the calculation of Rodriguez et al. [22] and the experimental data of Hippler et al. [38].

The excitation cross sections for the $1s \rightarrow 2p$ transition obtained with proton and antiproton projectiles are shown in Figure 3.5 as a function of projectile energy, in comparison with other theoretical calculations and experimental and recommended data (for proton impact). In this case, our TDCC method yields slightly lower values than the recommended and experimental values for protons, as well as for both theoretical calculations for antiprotons, at all energies. However, for proton projectiles the present TDCC results are in good agreement with the recent convergent close-coupling (CCC) calculations of Alladustov et al. [23]. This is not a surprise since both approaches use a relatively large basis set during the solution of the time-dependent Schrödinger equation. In contrast, there is noticeable difference between the present TDCC results and previous calculations [27, 28] for antiprotons, which can be attributed to the smaller basis sets used in those calculations. Our perturbational results are higher than the TDCC ones for both projectiles. While these results show good agreement with other theories for antiprotons and with experimental data for protons above a projectile energy of 500 keV, they overestimate all other data below this energy.

The excitation cross sections calculated for the $1s \rightarrow 3d$ transition are presented in Figure 3.6, in comparison with the available recommended and experimental values for proton impact, and theoretical calculations for antiproton impact. In the case of protons, the TDCC results agree well with the recommended values for energies above 500 keV. For the low energies (below 200 keV), there is a good agreement with the experimental data of Van den Bos et al. [39]. Here, the recommended values are lower. In contrast to the other two excitations, in this case the first-order results are lower than the ab initio ones. In the case of antiprotons, our TDCC results are lower than those of the other two calculations of Igarashi et al. [27] and McGovern et al. [28]. Surprisingly, our first-order results are in perfect agreement with the ab initio ones above 250 keV. Below this energy, however, the first-order calculations underestimate the TDCC results.

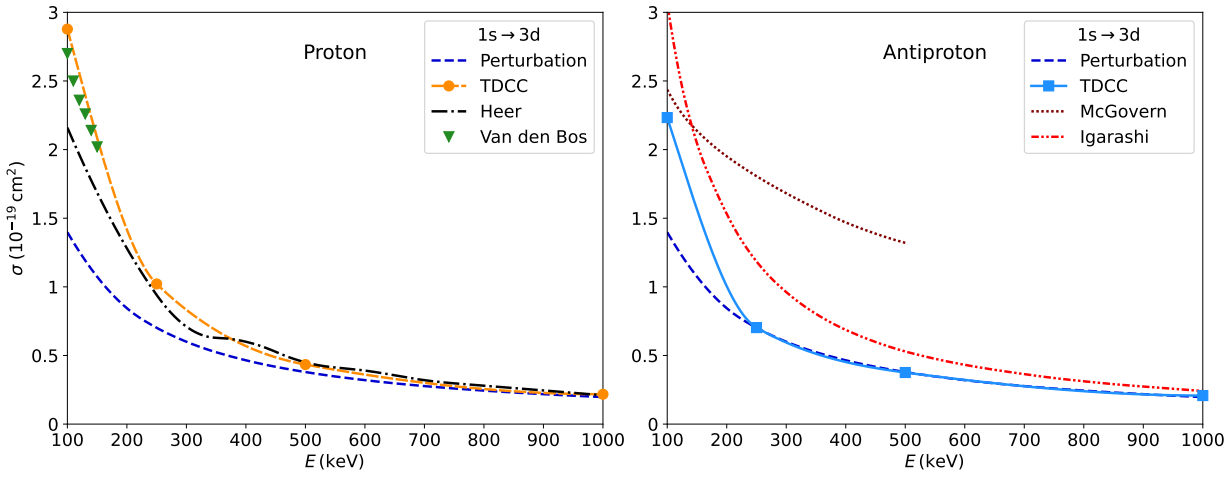

Figure 3.6: Same as Figure 3.4, but for the $1s \rightarrow 3d$ transition. The results for protons are compared in addition to the experimental results of Van den Bos et al. [39].

Finally, in Figure 3.7, we present a comparison of the excitation cross sections for proton and antiproton projectiles obtained using the TDCC method and the first-order approximation for all three excited states studied. One may observe that, for the excitation of the $2p$ state, the cross sections for protons and antiprotons are almost identical. This does not mean that higher-order effects are not important; as we have seen in Figure 3.2, transition probabilities depending on the impact parameter differ for the two projectiles. For this excitation, the effects for small and large impact parameters cancel each other out. The first-order perturbational results overestimate the TDCC ones for all energies, especially on the lower side. In the case of the other two studied excitations' cross sections, the results for protons are comparatively higher than those for antiproton projectiles. As expected, the difference increases for lower impact energies, because here, higher-order effects, responsible

for the Barkas effect, are more important. The perturbational results reproduce the TDCC cross sections for the excitation of the $2s$ state by proton impact almost exactly, and for the excitation of the $3d$ they are in very good agreement with the TDCC results for antiprotons above 250 keV. Looking at Figures 3.1–3.3, this agreement is also a result of the cancellation of differences in transition probabilities for small and large impact parameters. It can be also observed, that the difference between proton and antiproton excitation cross sections is significantly larger in the case of dipole-forbidden transitions compared to the dipole-allowed transitions. This behaviour was also observed in the case of the H target [8].

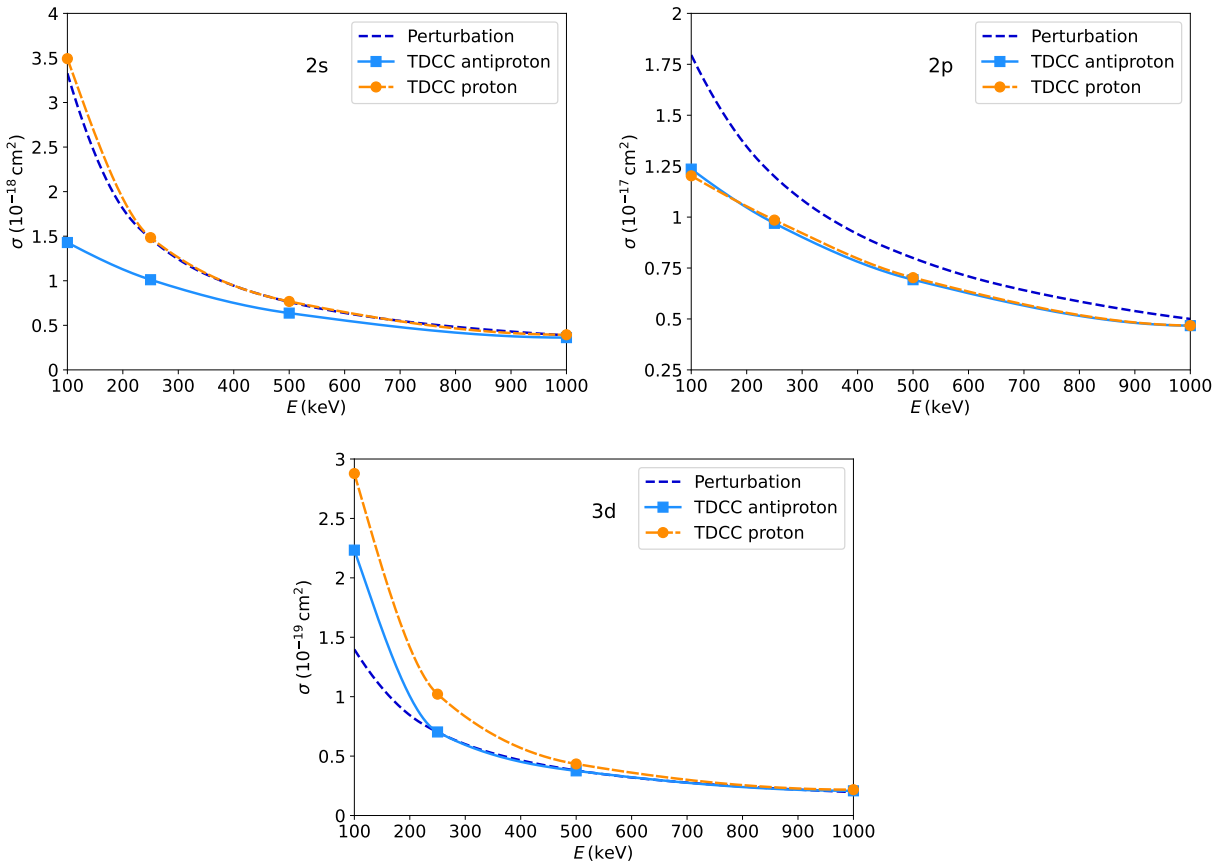

Figure 3.7: Comparison of excitation cross sections for helium, obtained using TDCC calculations for proton and antiproton projectiles, and the perturbational approximation. Excitation to the $2s$, $2p$ and $3d$ states are presented as a function of projectile energy.

Conclusions

We have performed perturbational and ab initio TDCC calculations for the excitation of helium by proton and antiproton impact. Studying the impact parameter dependence of the transition probabilities, we have observed that these behave differently for the three studied excitations. For the $2s$ state transition, the probabilities for antiprotons are higher relative to protons for all impact parameters. In the case of the excitation of the $2p$ and $3d$ states for small impact parameters, the transition probabilities for antiproton projectiles are higher, while for larger impact parameters the proton projectiles induce the transition with a higher probability.

Concerning the excitation cross sections as a function of the impact energy, the results for proton and antiproton projectiles are practically equal for the highest considered energy, 1000 keV. This suggests that higher-order effects, responsible for the dependence of the cross section on the projectile charge sign, can be neglected in this case. Consequently, the first-order perturbational calculations reproduce the TDCC results well at this energy. For lower impact energies, in the case of the excitation of the $2s$ and $3d$ states, higher cross sections are obtained for protons than for antiprotons. For the excitation of the $2p$ state, the cross sections obtained with proton and antiproton projectiles are almost the same. Concerning the perturbational results, these overestimate the TDCC ones for the $2p$ state, while in the case of $2s$ they reproduce the cross sections obtained with protons almost exactly. As for the $3d$ state, the perturbational result is below the TDCC ones for the lowest impact energy (100 keV), while for higher energies follow the TDCC data for antiprotons.

Comparing our results with other calculations, and in the case of the proton impact on the recommended and experimental cross sections (excitation of the $2s$), the agreement is very good. In other cases, such as the excitation of the $2p$ state by proton impact, our TDCC results are in good agreement with other elaborate calculations [23], but are below the experimental and recommended cross sections. For the excitation of the $3d$ state with the same projectile, the agreement with the experimental data (small impact energies) or

the recommended values (higher energies) is good. In case of the excitation of the $2p$ and $3d$ states by antiproton projectiles, our TDCC results are below the other two available calculations, which can be attributed to the relatively small configuration space on which the Schrödinger equation was solved in those studies.

Appendix A

Perturbation Theory

The derivation of the first-order perturbation approximation presented here is based on [40].

Suppose that the time-dependent Hamiltonian of the system can be written in the form:

$$H(t) = H^{(0)} + V(t), \tag{A.1}$$

where $H^{(0)}$ is the time-independent unperturbed Hamiltonian, and $V(t)$ is the time-dependent perturbation potential. The eigenstates and eigenvalues of $H^{(0)}$ are known.

The evolution of the atomic system is described in the Schrödinger picture by the evolution operator $U(t, t_0)$. The evolution operator is defined by the following integral equation, which is equivalent to the Schrödinger equation:

$$U(t, t_0) = 1 - i \int_{t_0}^{t} H(\tau) U(\tau, t_0) d\tau \tag{A.2}$$

and the initial condition

$$U(t_0, t_0) = 1. \tag{A.3}$$

The $U(t, t_0)$ evolution operator is unitary

$$U(t, t_0) U^{\dagger}(t, t_0) = U^{\dagger}(t, t_0) U(t, t_0) = 1. \tag{A.4}$$

It also satisfies the composition property

$$U(t_2, t_0) = U(t_2, t_1) U(t_1, t_0), \; t_2 > t_1 > t_0. \tag{A.5}$$

The evolution operator corresponding to the $H^{(0)}$ operator is defined as:

$$U^{(0)}(t,\ t_0) = 1 - i\int_{t_0}^{t} H^{(0)}(\tau)U^{(0)}(\tau,t_0)d\tau, \tag{A.6}$$

$$U^{(0)}(t_0,t_0) = 1. \tag{A.7}$$

Since $H^{(0)}$ is independent of time, the solution has the form:

$$U^{(0)}(t,t_0) = \exp\left[-iH^{(0)}(t-t_0)\right]. \tag{A.8}$$

Using $U^{(0)}(t,t_0)$ we can write the evolution operator for the states in the interaction picture:

$$U_I(t,t_0) = U^{(0)^\dagger}(t,t_0)U(t,t_0), \tag{A.9}$$

which satisfies the equations:

$$U_I(t,\ t_0) = 1 - i\int_{t_0}^{t} V_I(\tau)U_I(\tau,t_0)d\tau, \tag{A.10}$$

$$U_I(t_0,t_0) = 1, \tag{A.11}$$

where

$$V_I(t) = U^{(0)^\dagger}(t,t_0)V(t)U^{(0)}(t,t_0). \tag{A.12}$$

The evolution operator in the interaction picture can be expanded as:

$$U_I(t,t_0) = 1 + \sum_{n=1}^{\infty} U_I^{(n)}(t,t_0), \tag{A.13}$$

$$U_I^{(n)}(t,t_0) = (-i)^n \int_{t>\tau_n>\tau_{n-1}>\ldots>\tau_1>t_0} d\tau_n d\tau_{n-1}\ldots d\tau_1 V_I(\tau_n)V_I(\tau_{n-1})\ldots V_I(\tau_1). \tag{A.14}$$

Transforming back to the Scrödinger picture results in the following expansion:

$$U(t,t_0) = U^{(0)}(t,t_0) + \sum_{n=1}^{+\infty} U^{(n)}(t,t_0), \tag{A.15}$$

$$\begin{aligned} U^{(n)}(t,t_0) = (-i)^n \int_{t>\tau_n>\tau_{n-1}>\ldots>\tau_1>t_0} & d\tau_n d\tau_{n-1}\ldots d\tau_1 U^{(0)}(t,\tau_n)V(\tau_n)\times \\ & \times U^{(0)}(\tau_n,\tau_{n-1})V(\tau_{n-1})\ldots U^{(0)}(\tau_2,\tau_1)V(\tau_1)U^{(0)}(\tau_1,t_0). \end{aligned} \tag{A.16}$$

Using (A.15) we can write the expansion for the transition amplitude:

$$a_{i\to f} = \langle f|U(t,t_0)|i\rangle = \sum_{n=1}^{\infty}\langle f|U^{(n)}|i\rangle. \tag{A.17}$$

The first-order amplitude can be expressed as follows:

$$\langle f|U^{(1)}|i\rangle = \int_{t_0}^{t} d\tau\, \langle f|e^{iH^{(0)}\tau}V(t)e^{-iH^{(0)}\tau}|i\rangle = \int_{t_0}^{t} d\tau\, e^{i(E_f-E_i)\tau}\langle f|V(t)|i\rangle. \tag{A.18}$$

The perturbation potential is the Coulomb interaction potential between the active electron and the projectile:

$$V(t) = -\frac{Z_p}{|\mathbf{R}(t)-\mathbf{r}|}. \tag{A.19}$$

Here $\mathbf{R}(t)$ is the position vector of the projectile and $\mathbf{r}$ is the position vector of the active electron. Z_p is the charge of the projectile.

The projectile's position vector can be decomposed into a component parallel to the projectile's trajectory and a component perpendicular to it.

$$\mathbf{R} = \mathbf{z} + \mathbf{b}, \tag{A.20}$$

$$R = \sqrt{z^2+b^2}. \tag{A.21}$$

Using the substitution $z = vt$, the first-order amplitude takes the following form:

$$a_{i\to f}^{(1)} = i\frac{Z_p}{v}\int_{-\infty}^{\infty} dz\, e^{i\frac{E_f-E_i}{v}z}\left\langle f\left|\frac{1}{|\mathbf{R}(t)-\mathbf{r}|}\right|i\right\rangle. \tag{A.22}$$

Finally, the first-order approximation of the cross section for the $i \to f$ transition can be calculated as follows:

$$\sigma_{i\to f}^{(1)} = \int d^2\mathbf{b}|a_{i\to f}^{(1)}(\mathbf{b})|^2 = \int d^2\mathbf{b}\, a_{i\to f}^{(1)*}(\mathbf{b})\, a_{i\to f}^{(1)}(\mathbf{b}). \tag{A.23}$$

Bibliography

[1] Bálint, Z.; Borbély, S.; Nagy, L. Excitation of Helium by Proton and Antiproton Impact. *Atoms* **2024**, *12*, 57.

[2] Thomas, E.W.; Bent, G.D. Formation of Excited States in a Helium Target by the Impact of 0.15- to 1.0-MeV Protons and Deuterons. I. Experimental. *Phys. Rev.* **1967**, *164*, 143–150.

[3] Thomas, E.W. Cross Sections for the Formation of Excited States in a Helium Target by the Impact of 0.15- to 1.0-MeV Protons and Deuterons. II. Comparison with Theory. *Phys. Rev.* **1967**, *164*, 151–155.

[4] Fritsch, W. Helium Excitation in Heavy Particle Collisions. In *Atomic and PlasmaMaterial Interaction Data for Fusion*; IAEA: Vienna, Austria, 1992; Volume 3, pp. 41–46.

[5] De Heer, F.; Hoekstra, R.; Summers, H.P.; Undertaking, J.J. New Assessment of Cross-Section Data for Helium Excitation by Protons. In *Atomic and PlasmaMaterial Interaction Data for Fusion*; IAEA: Vienna, Austria, 1992; Volume 3, pp. 47–50.

[6] Andersen, L.H.; Hvelplund, P.; Knudsen, H.; Moller, S.P.; Sorensen, A.H.; Elsener, K.; Rensfelt, K.-G.; Uggerhoj, E. Multiple ionization of He, Ne, and Ar by fast protons and antiprotons. *Phys. Rev. A* **1987**, *36*, 3612-3629.

[7] Reading, J.F.; Ford, A.L. The forced impulse method applied to the double ionisation of helium by collision with high-energy protons, antiprotons and alpha particles. *J. Phys. B Atom. Mol. Phys.* **1987**, *20*, 3747–3769.

[8] Knudsen, H.; Reading, J. Ionization of atoms by particle and antiparticle impact. *Phys. Rep.* **1992**, *212*, 107–222.

[9] Nagy, L. Two-electron processes in fast collisions with charged particles. *Nucl. Instrum. Methods Phys. Res. B* **1997**, *124*, 271–280.

[10] Andersen, L.H.; Hvelplund, P.; Knudsen, H.; Mo, S.P.; Pedersen, J.O.P.; Tang-Petersen, S.; Uggerho, E.; Elsener, K.; Morenzoni, E. Single ionization of helium by 40–3000-keV antiprotons. *Phys. Rev. A* **1990**, *41*, 6536–6539.

[11] Hvelplund, P.; Knudsen, H.; Mikkelsen, U.; Morenzoni, E.; Moller, S.P.; Uggerhoj, E.; Worm, T. Ionization of helium and molecular hydrogen by slow antiprotons. *J. Phys. B At. Mol. Opt. Phys.* **1994**, *27*, 925.

[12] Knudsen, H.; Kristiansen, H.-P.E.; Thomsen, H.D.; Uggerhøj, U.I.; Ichioka, T.; Møller, S.P.; Hunniford, C.A.; McCullough, R.W.; Charlton, M.; Kuroda, N.; et al. Ionization of Helium and Argon by Very Slow Antiproton Impact. *Phys. Rev. Lett.* **2008**, *101*, 043201.

[13] Knudsen, H.; Kristiansen, H.-P.E.; Thomsen, H.D.; Uggerhøj, U.I.; Ichioka, T.; Møller, S.P.; Hunniford, C.A.; McCullough, R.W.; Charlton, M.; Kuroda, N.; et al. On the double ionization of helium by very slow antiproton impact. *Nucl. Instrum. Methods Phys. Res. Sect. B* **2009**, *267*, 244.

[14] Khayyat, K.; Weber, T.; Dörner, R.; Achler, M.; Mergel, V.; Spielberger, L.; Jagutzki, O.; Meyer, U.; Ullrich, J.; Moshammer, R.; et al. Differential cross sections in antiproton- and proton-helium collisions. *J. Phys. B At. Mol. Opt. Phys.* **1999**, *32*, L73.

[15] Kirchner, T.; Knudsen, H. Current status of antiproton impact ionization of atoms and molecules: Theoretical and experimental perspectives. *J. Phys. B At. Mol. Opt. Phys.* **2011**, *44*, 122001.

[16] Pindzola, M.S.; Lee, T.G.; Colgan, J. Antiproton-impact ionization of H, He and Li. *J. Phys. B At. Mol. Opt. Phys.* **2011**, *44*, 205204.

[17] Guan, X.; Bartschat, K. Complete Breakup of the Helium Atom by Proton and Antiproton Impact. *Phys. Rev. Lett.* **2009**, *103*, 213201.

[18] Abdurakhmanov, I.B.; Kadyrov, A.S.; Fursa, D.V.; Bray, I.; Stelbovics, A.T. Convergent close-coupling calculations of helium single ionization by antiproton impact. *Phys. Rev. A* **2011**, *84*, 062708.

[19] Foster, M.; Colgan, J.; Pindzola, M.S. Fully Correlated Electronic Dynamics for Antiproton Impact Ionization of Helium. *Phys. Rev. Lett.* **2008**, *100*, 033201.

[20] Borbély, S.; Feist, J.; Tőkési, K.; Nagele, S.; Nagy, L.; Burgdörfer, J. Ionization of helium by slow antiproton impact: Total and differential cross sections. *Phys. Rev. A* **2014**, *90*, 052706.

[21] Borbély, S.; Tong, X.-M.; Nagele, S.; Feist, J.; Bezinová, I.; Lackner, F.; Nagy, L.; Tőkési, K.; Burgdörfer, J. Electron correlations in the antiproton energy-loss distribution in He. *Phys. Rev. A* **2018**, *98*, 012707.

[22] Rodríguez, V.D.; Ramírez, C.A.; Rivarola, R.D.; Miraglia, J.E. Helium excitation by protons and highly-charged-ion impact. *Phys. Rev. A* **1997**, *55*, 4201-4208.

[23] Alladustov, S.U.; Abdurakhmanov, I.B.; Kadyrov, A.S.; Bray, I.; Bartschat, K. Wave-packet continuum-discretization approach to proton collisions with helium. *Phys. Rev. A* **2019**, *99*, 052706.

[24] Spicer, K.H.; Plowman, C.T.; Abdurakhmanov, I.B.; Kadyrov, A.S.; Bray, I.; Alladustov, S.U. Differential study of proton-helium collisions at intermediate energies: Elastic scattering, excitation, and electron capture. *Phys. Rev. A* **2021**, *104*, 032818.

[25] Hall, K.A.; Reading, J.F.; Ford, A.L. Excitation and ionization of atomic hydrogen by antiprotons. *J. Phys. B* **1996**, *29*, 6123.

[26] Kirchner, T.; Lüdde, H.J.; Kroneisen, O.J.; Dreizler, R.M. New trends in the description of ionatom collisions by time-dependent quantum methods. *Nucl. Instrum. Methods Phys. Res. B* **1999**, *154*, 46–53.

[27] Igarashi, A.; Ohsaki, A.; Nakazaki, S. Single ionization of helium by antiproton impact. *Phys. Rev. A* **2000**, *62*, 052722.

[28] McGovern, M.; Assafrão, D.; Mohallem, J.R.; Whelan, C.T.; Walters, H.R.J. Differential and total cross sections for antiproton-impact ionization of atomic hydrogen and helium. *Phys. Rev. A* **2009**, *79*, 042707.

[29] Nagy, L., Tóth, I. and Campeanu, R.I. Electron and Positron Impact Ionization of Molecules. *Atoms* **2024**, *12*, 38

[30] Schneider, B.I.; Collins, L.A. The discrete variable method for the solution of the time-dependent Schrödinger equation. *J. -Non-Cryst. Solids* **2005**, *351*, 1551–1558.

[31] Rescigno, T.N.; McCurdy, C.W. Numerical grid methods for quantum-mechanical scattering problems. *Phys. Rev. A* **2000**, *62*, 032706.

[32] Park, T.J.; Light, J.C. Unitary quantum time evolution by iterative Lanczos reduction. *J. Chem. Phys.* **1986**, *85*, 58705876.

[33] Schneider, B.I.; Feist, J.; Nagele, S.; Pazourek, R.; Hu, S.; Collins, L.A.; Burgdörfer, J. Recent Advances in Computational Methods for the Solution of the Time-Dependent Schrödinger Equation for the Interaction of Short, Intense Radiation with One and Two Electron Systems. In *Quantum Dynamic Imaging: Theoretical and Numerical Methods*; Bandrauk, A.D., Ivanov, M., Eds.; Springer: New York, NY, USA, 2011; pp. 149–208.

[34] Hernandez, V.; Roman, J.E.; Vidal, V. SLEPc: A scalable and flexible toolkit for the solution of eigenvalue problems. *ACM Trans. Math. Softw.* **2005**, *31*, 351–362.

[35] Nesbet, R.K.; Watson, R.E. Approximate Wave Functions for the Ground State of Helium. *Phys. Rev.* **1958**, *110*, 1073–1076.

[36] Bransden, B.H.; Joachain, C.J. *Physics of Atoms and Molecules*; Longman & Scientific Technical: New York, NY, USA, 1983; pp. 139, 275, 285.

[37] Bohr, N., II. On the theory of the decrease of velocity of moving electrified particles on passing through matter. *Philos. Mag.* **1913**, *25*, 10–31.

[38] Hippler, R.; Schartner, K.H. Absolute cross sections for the excitation of n^1P-levels of helium by proton impact (150–1000 keV). *J. Phys. B Atom. Mol. Phys.* **1974**, *7*, 618.

[39] Van den Bos, J.; Winter, G.J.; De Heer, F.J. Excitation of helium by protons in the 1150 keV region. *Physica* **1968**, *40*, 357–384.

[40] Messiah, A. Approximate Solutions of the Time-Dependent Schrödinger Equation. In *Quantum Mechanics*; North Holland Publishing Company: Amsterdam, Netherlands, 1962; Volume 2, pp. 722–725.